

Ising models on the hydrogen peroxide and other lattices

Xiaofeng Qian^{a,*}, Youjin Deng^b, Lev N. Shchur^{c,d}, Henk W. J. Blöte^a

^a*Lorentz Institute, Leiden University, P.O. Box 9506, Leiden, 2300 RA, The Netherlands*

^b*University of Science and Technology of China, Hefei, 230027, China*

^c*Laboratory for Computational Physics, HSE University, Moscow, 123458, Russia*

^d*Landau Institute for Theoretical Physics, Chernogolovka, 142432, Russia*

Abstract

We perform a Monte Carlo analysis of the Ising model on many three-dimensional lattices. By means of finite-size scaling we obtain the critical points and determine the scaling dimensions. As expected, the critical exponents agree with the three-dimensional Ising universality class for all models. The irrelevant field, as revealed by the correction-to-scaling amplitudes, appears to be relatively large. Combining the Monte Carlo results for the hydrogen peroxide lattice with those for five other three-dimensional lattices, we obtain a set of data covering a wide range of the irrelevant temperature field. This is helpful in the determination of the parameters describing the corrections to scaling. As a consequence, new results are obtained for the universal parameters describing Ising criticality in three dimensions, with reduced error margins in comparison with earlier Monte Carlo analyses. The critical exponents describing the thermodynamic singularities are determined by the temperature renormalization exponent $y_t = 1.58693(9)$ and the magnetic renormalization exponent $y_h = 2.48178(5)$. The corrections to scaling are governed by the irrelevant exponent $y_1 = -0.821(5)$.

Keywords: continuous phase transitions, critical exponents, universality class, three-dimensional Ising model, Monte Carlo simulation, finite-size scaling

1. Introduction

The universality class of the three-dimensional Ising model covers a wide range of models and systems with short-range interactions and a scalar order parameter. Among these, the critical points of simple gas-liquid systems may be considered the most common ones. It is thus appropriate to formulate theoretical approaches to describe the phase transitions of this type. In

*Corresponding author. Email: xfqian272@hotmail.com

Email addresses: yjdeng@ustc.edu.cn (Youjin Deng), lshchur@hse.ru (Lev N. Shchur)

the absence of exact solutions, many efforts have been made to obtain the universal constants of this class as accurately as possible. The development of the renormalization theory [1] did not only yield more and new insight in phase transitions, but also accurate results for the universal exponents; see Refs. [2, 3] and references therein. Furthermore, the increasing number of terms in series expansions of the Ising model enables increasingly accurate estimates of these exponents, see e.g., Ref. [4] and references therein. In a different type of approach, the recent availability of fast and relatively cheap computers has opened the possibility to obtain similarly accurate estimates by means of Monte Carlo simulations and finite-size scaling, see e.g., Ref. [5] and references therein. Since the latter approach will also be the subject of the present work, we outline the ideas behind it. The finite-size scaling behavior of observables such as the specific heat, susceptibility etc. at criticality is typically described by divergences according to power laws modified by corrections to scaling. In first order, these corrections are proportional to the irrelevant renormalization fields that parametrize the critical subspace of the Ising model. The presence of such corrections naturally leads to a reduction of the accuracy of the determination of the universal parameters. The numerical analysis of such a correction requires the determination of its amplitude as well as of the associated irrelevant exponent. These corrections are usually important, and neglecting them has yielded incorrect results [6, 7, 8].

While an accurate determination of the irrelevant exponent would favor the use of an Ising model with a relatively large correction amplitude, i.e., a large irrelevant field, a problem may arise in the accuracy of the numerical analysis because the quadratic term in the irrelevant scaling field may become important, thus affecting the accuracy of the determination of the irrelevant exponent and other universal parameters. A model with a small irrelevant field can well be used to determine the other universal parameters, at least if the irrelevant exponent is approximately known. However, such a model is obviously not suitable to determine the irrelevant exponent.

The strategy followed in Ref. [5, 9] therefore relied on the simultaneous analysis of several models, with considerably different irrelevant fields. The availability of such Monte Carlo-generated finite-size data enables an analysis that can be done in two stages, the first of which is to check whether the data for the different models are consistent with universality. Then, the second stage, which is based on the assumption that universality is *exactly* satisfied, combines

the relevant Monte Carlo data for all models and applies a fitting procedure in which the universal parameters occur only once.

The choice of the models is based on the observed dependence of the correction-to-scaling amplitudes on further-neighbor interactions [10] and on the introduction of a vacant spin state as specified by the Blume-Capel model [11, 12]. The effects of interactions with further neighbors on the irrelevant field can be understood in terms of the crossover between the long-range mean-field fixed point and the short-range Ising fixed point [13]. This explains why the variation of the number of interacting neighbors has a strong effect on the correction-to-scaling amplitudes. Furthermore the relation between the activity of the vacancies (spin-zero states) and the irrelevant field, which was described in the renormalization analysis of the Potts model by Nienhuis et al. [14], explains the behavior of the correction amplitudes in the Blume-Capel model.

The range of irrelevant fields between the Ising and mean-field fixed points is simply accessible by adjusting the number of interacting neighbors. But the range of irrelevant fields on the other side of the Ising fixed point is less easy to explore. In principle, that range of irrelevant fields can be accessed by introducing antiferromagnetic interactions with further neighbors. However, a sufficiently efficient algorithm for the simulation of such models is not available, and we will focus instead on individual models that are known or expected to lie in the desired range. One of these is the simple-cubic lattice gas [5] with nearest-neighbor exclusions, but it is difficult to obtain the same level of statistical accuracy as for other models. We thus select another Ising model with few interacting neighbors, namely the model on the hydrogen peroxide lattice, with coordination number three. On this basis we expect that the irrelevant field will even exceed (in absolute value) that of the Ising model on the diamond lattice [5] which has coordination number four.

In addition to the study of the model on the hydrogen peroxide lattice, the present paper reconsiders five of the models of Ref. [5] and adds new simulation results for system size $L = 256$, as well as results for smaller systems with improved statistics. Our intention is not only to narrow down the statistical error margins, but also to obtain data for a wide range of values of the irrelevant field. Subsequent analysis will purportedly improve our knowledge of the universal parameters.

The outline of the next sections is as follows. Section 2 defines the six models and the

simulation methods, and supplies some further details on the simulations and the computational resources. Part of the data for the nearest-neighbor Ising model were generated by the Cluster Processor [15]. We include a subsection on this special-purpose computer. Section 3 provides finite-size scaling analyses for the six models separately, and the results are subjected to a consistency test with universality. An analysis of the Ising universal parameters by means of a simultaneous fitting procedure is performed in Sec. 4. A short discussion in Sec. 5 concludes this paper.

2. Models and computational resources

2.1. The model on the hydrogen peroxide lattice

The spin- $\frac{1}{2}$ Ising model is described by the reduced Hamiltonian

$$\mathcal{H}/k_B T = -K \sum_{\langle ij \rangle} s_i s_j, \quad (1)$$

where the spins s_i are labeled by the lattice site number i . They are normalized such as to assume values ± 1 , and are located on the vertices of the hydrogen peroxide lattice, which is shown in Fig. 1. The spins interact with only three of their neighbors, as shown by the solid lines in the figure. The lattice has cubic symmetry, so that the three main crystal axes are equivalent. The critical point of the Ising model on the hydrogen peroxide lattice has been determined by means of series expansions by Leu et al. [16] as $K_c = 0.573795(16)$. This Ising model is interesting because of the low coordination number and the expected special value of the irrelevant field, and the equivalence with a nonintersecting-loop model [17]. However, as far as we were able to check, no further research on this model has been reported.

2.2. Other models, simulations and random-number generator

In addition to the model on the hydrogen peroxide lattice, which we label as model 1, the present Monte Carlo analysis includes five more Ising-like models. They can be defined in terms of the following spin-1 Hamiltonian

$$\mathcal{H}/k_B T = -K \sum_{i < j} \theta(R - r_{ij}) s_i s_j + D \sum_k (s_k^2 - 1), \quad (2)$$

where the sums are over the sites of the diamond lattice (model 2), or the simple-cubic lattice (models 3-6). The lattice sites are labeled by i, j and k . The distance between sites i and j is

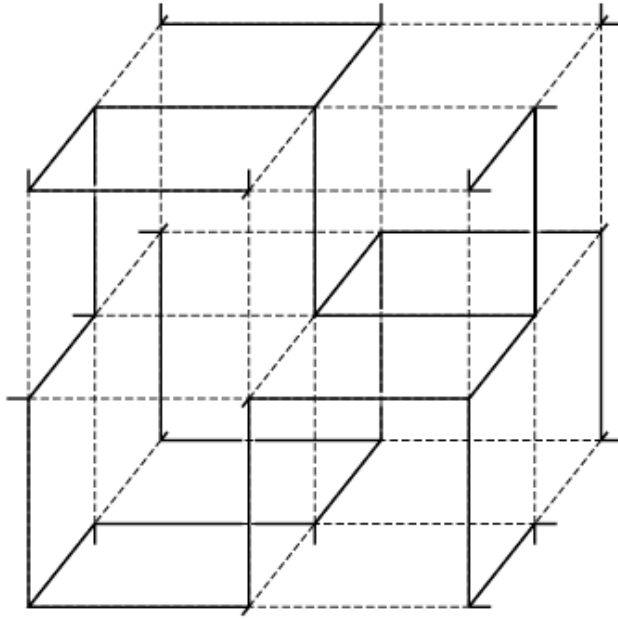


Figure 1: Sketch of the hydrogen peroxide lattice. The Ising spins are located at the vertices of the lattice. Each spin interacts with three nearest neighbors. The nearest-neighbor couplings are shown as solid lines. The hydrogen peroxide lattice has cubic symmetry, and all sites are equivalent. In this sketch, the lattice sites coincide with those of the simple cubic lattice, but the number of spin-spin couplings is less by a factor of two.

denoted r_{ij} , and the step function $\theta(x)$, which is equal to 0 for $x < 0$ and equal to 1 for $x \geq 0$, defines a cutoff of the interactions of strength K at range R . The ranges R are chosen such that interactions are restricted to the four nearest neighbors (model 2), six nearest neighbors (models 3 and 4), 26 closest neighbors (model 5), or the 32 closest neighbors (model 6). The spins can assume the values $s_i = \pm 1$ or 0. However, for models 1, 2, and 3 the parameter D is set to the value $D = -\infty$ so that the $s_i = 0$ state is excluded, and the model in effect reduces to the spin- $\frac{1}{2}$ model. For model 4, we take $D = \ln 2$ which leads to a system with strongly reduced corrections to scaling [9]; moreover, the model can be mapped on a spin- $\frac{1}{2}$ model, which allows efficient simulations by means of a cluster algorithm [9]. A newer algorithm does not use the spin- $\frac{1}{2}$ representation and applies cluster steps directly to spins 1, which include transitions between spin-1 and 0 states [5] without the need to include local updates by Metropolis steps. Further details about the algorithms, also describing how models 5 and 6 can be efficiently simulated, appear in Ref. [5]. It is noteworthy that it is possible to apply the star-triangle transformation to model 1, which leads to another Ising model with only half the number of spins, which may thus enable somewhat faster simulations. Since the data sampling would then

become more time-consuming, we have chosen to simulate the original model on the hydrogen peroxide lattice.

Table 1: Description of the six simulated Ising models. The abbreviation “# nb.” stands for neighbor spins coupled to each spin.

model	D	lattice	spin	# nb.
1	∞	hydr. peroxide	spin- $\frac{1}{2}$	3
2	∞	diamond	spin- $\frac{1}{2}$	4
3	∞	simple cubic	spin- $\frac{1}{2}$	6
4	$\ln 2$	simple cubic	spin-1	6
5	∞	simple cubic	spin- $\frac{1}{2}$	26
6	∞	simple cubic	spin- $\frac{1}{2}$	32

The definitions of the six models are summarized in Table 1. For the models on the simple cubic lattice, the unit cell contains one site and the finite-size parameter L is thus equal to the size of the periodic box, expressed in nearest-neighbor distances. The unit cells of the hydrogen peroxide and the diamond lattices can be chosen as cubes containing eight sites.

It is thus convenient to assign a size 2 to these unit cells, so that a system of size L contains L^3 spins, just as the models on the simple cubic lattice. Expressed in these units, the nearest-neighbor distances are however $1/2$ and $\sqrt{3}/2$ respectively. Using a cubic cell of size 2, the positions modulo 2 of the spins on the diamond lattice are $(0, 0, 0)$, $(1, 1, 0)$, $(1, 0, 1)$, $(0, 1, 1)$, $(\frac{1}{2}, \frac{1}{2}, \frac{1}{2})$, $(\frac{3}{2}, \frac{3}{2}, \frac{1}{2})$, $(\frac{3}{2}, \frac{1}{2}, \frac{3}{2})$, $(\frac{1}{2}, \frac{3}{2}, \frac{3}{2})$.

The Monte Carlo simulations used systems of size $L \times L \times L$ with periodic boundary conditions, and system sizes in the range $4 \leq L \leq 256$. The bulk of the simulations took place very close to the known critical points [5]. A small fraction of the computer time was spent on simulations somewhat further away from the critical point, in order to determine the temperature-dependences of the sampled quantities for some smaller systems $L \leq 32$. Table 2 presents the number of ten millions of samples taken per system size and the number of simulation sweeps before taking each sample. The system sizes were taken in the range $4 \leq L \leq 256$.

Since very long computer runs are impractical, we divided the simulations for a specified

Table 2: Number of samples (in ten millions) and simulation steps per sample for each model. We use the notation $M \times N$ to indicate that $10^7 M$ samples have been taken at intervals of N single-cluster steps. Smaller even system sizes $4 \leq L \leq 18$ are also included in the simulations. Odd systems $5 \leq L \leq 15$ were simulated where possible, i.e., for models 3, 4, 5, and 6. At least 200×10^7 samples were taken for the smaller system sizes $L < 20$.

model \ L	20	22	24	28	32	40	48	64	128	256
1	200×5	200×6	200×6	200×7	200×8	240×10	200×12	120×16	24×32	4.0×64
2	220×10	220×10	260×10	280×10	300×10	600×10	160×20	140×20	20×40	4.0×64
3	200×10	200×11	320×12	200×14	240×16	240×20	120×24	120×32	20×64	3.6×128
4	200×6	200×6	200×6	160×6	160×8	140×10	100×12	80×16	24×32	3.0×64
5	200×20	120×22	120×24	120×28	120×32	140×40	100×48	60×64	16×128	3.0×256
6	200×20	120×22	120×24	120×28	120×32	120×40	100×48	60×64	16×128	3.0×256

model, system size and coupling into many independent runs. The total number of runs was over 8000. Next, the data for a given model, system size and coupling were combined into an average on the basis of their individual standard deviations. These standard deviations were obtained from a partitioning of each run into two thousand subruns and subsequent statistical analysis.

During this step of data compression, we discarded four runs that displayed unacceptable deviations (over four standard deviations) from the average. Some of the discarded runs could be traced back to the same computer which was thus diagnosed to be defective.

Much attention is needed in order to obtain Monte Carlo results free of biases due to imperfect random number generators. This means actually that such biases must be reduced to a level that is small in comparison with the statistical uncertainties. In this work we employ pseudo-random-number generators based on binary shift registers. It is known that such pseudo-random-numbers are not sufficiently random for some purposes. Significant errors were reported (see, e.g., Refs. [18, 19, 20, 21, 22, 23, 24, 25, 26, 27]). In many applications, the deviations from randomness are dominated by three-bit correlations which are a direct consequence of the production rule.

In order to avoid systematic effects we have to deal with the problem that the present

simulations are of a considerable length, and we wish to avoid tests with a similar magnitude. For this reason we make use of the “scalability” of the biases as reported earlier for cluster simulations [25, 26]. On this basis we can extrapolate the biases found for smaller systems and shorter shift registers to estimate the bias effects in our simulations. Additional confidence in the validity of our approach is based on the observation [25] that the magnitude of the observed biases decreases rapidly as a function of the number of correlated bits. By modulo-2 addition of two maximum-length shift registers with a three-bit production rule, it is possible to form a new sequence whose dominant correlation is a nine-bit one, which does almost satisfy the maximum-length criterion. On the basis of the aforementioned extrapolations [25, 26], we believe that this procedure suppresses the biases below the present threshold of observability.

2.3. The cluster processor

The preparations for the construction of the Cluster Processor started in 1992. The plan was to construct one prototype processor and, after verification of its performance, to build a system of twelve parallel units for the Wolff simulation [28] of the three-dimensional Ising model with linear sizes up to $L = 256$. The first stage of this project, the construction of the prototype processor, was completed successfully in the expert hands of Dr. A. L. Talapov, who acted as the hardware specialist. The Monte Carlo data generated by this processor led to a few publications [15, 29, 30]. Four of the twelve processors could be made operational [31]. In spite of the delay and the less than projected capacity of the system, fairly accurate results for the three-dimensional Ising universal quantities could be obtained [32]. The data generated by it contribute significantly to the numerical data for model 3 analyzed in the present work. For the largest system size $L = 256$ it contributed about one third of the data for model 3, for $L = 128$ about one sixth.

3. Separate finite-size analyses

3.1. Dimensionless ratio Q

During the simulations, the magnetization density m was sampled, as well as its second moment $\langle m^2 \rangle$ and its fourth moment $\langle m^4 \rangle$. From these data we derived the ratio $Q = \langle m^2 \rangle^2 / \langle m^4 \rangle$, which is related to the Binder cumulant [33, 34], and tends to a universal constant at criticality. The analysis of Q formulated here is based on renormalization arguments. Since both $\langle m^2 \rangle$

and $\langle m^4 \rangle$ can be expressed in terms of derivatives of the free energy to the magnetic field, the scaling of the free energy yields the scaling behavior of Q near the critical point. Since the geometric factors, which contain the derivative of the magnetic scaling field to the physical magnetic field coupled to m , cancel between the numerator and denominator of Q , the zeroth order term in Q is dimensionless. The finite-size-scaling behavior of Q of the j -th model follows by including the finite-size parameter L in the free energy, taking the appropriate derivatives, and renormalization to finite size 1, as

$$Q(t, u_j, L) = \tilde{Q}(L^{y_t}t, L^{y_1}u_j) + \sum_k b_{k,j}L^{y_k}. \quad (3)$$

The temperature field which is denoted t , and the irrelevant field denoted u_j , are dependent on the nonuniversal parameters appearing in the Hamiltonian Eq. (2), while the function \tilde{Q} and the exponents y_t and y_1 are universal. A few correction terms on the right are included, of which one is due to the analytic background term in the second derivative of the free energy to the magnetic field, whose leading term is of order L^{2y_h-d} , where $d=3$ is the dimensionality and y_h is the magnetic renormalization exponent. This effect leads to a correction exponent $y_2=d-2y_h$. Furthermore the temperature scaling field may depend in second order on the physical magnetic field, so that higher order derivatives of the free energy to the magnetic field will include corrections with finite-size exponent $y_3=y_t-2y_h$. In order to bring Eq. (3) in a suitable form to describe Monte-Carlo generated finite-size data for Q , we expand the parameters t and u in the physical fields, namely the couplings K_j :

$$\begin{aligned} t &= a_j(K_j - K_{cj}) + c_j(K_j - K_{cj})^2 + \dots \\ u &= u + v_j(K_j - K_{cj}) + \dots, \end{aligned} \quad (4)$$

where K_{cj} is the critical point of the j -th model. The coefficients are nonuniversal and also carry a label indicating the model. The universal function \tilde{Q} is expanded as

$$\begin{aligned} \tilde{Q}(L^{y_t}t, L^{y_1}u) &= Q^{(0,0)} + L^{y_t}tQ^{(1,0)} + L^{2y_t}t^2Q^{(2,0)} + \\ &+ L^{3y_t}t^3Q^{(3,0)} + L^{4y_t}t^4Q^{(4,0)} + \dots \\ &+ L^{y_1}uQ^{(0,1)} + L^{2y_1}u^2Q^{(0,2)} + \dots \\ &+ L^{y_t+y_1}tuQ^{(1,1)} + \dots, \end{aligned} \quad (5)$$

where the superscripts of the expansion coefficients $Q^{(k,l)}$ denote derivatives of \tilde{Q} to its arguments. They are thus universal. Combination of Eq. (3) and the two expansions yields, Eqs. (4)

and (5), a result of which the leading terms are

$$\begin{aligned}
Q &= Q^{(0)} + q_{1j}(K_j - K_{cj})L^{y_t} + q_{2j}(K_j - K_{cj})^2L^{2y_t} + \\
&+ q_{3j}(K_j - K_{cj})^3L^{3y_t} + q_{4j}(K_j - K_{cj})^4L^{4y_t} + \\
&+ c_j(K_j - K_{cj})^2L^{y_t} + b_{1j}L^{y_1} + b_{2j}L^{y_2} + b_{3j}L^{y_3} + \\
&+ d_j(K_j - K_{cj})L^{y_t+y_1},
\end{aligned} \tag{6}$$

where we abbreviated $Q^{(0,0)}$ as $Q^{(0)}$. The constants q_{ij} are the product of universal and nonuniversal constants from both expansions. These as well as other free parameters in Eq. (6) were estimated by means of least-squares fits to the Monte Carlo data, for each of the six models. Our first aim is now to determine the universal quantity $Q^{(0)}$. To this purpose we set $y_1=-0.82(3)$, $y_2=-1.963(3)$, and $y_3=-3.375(3)$ as already specified in earlier analyses of Q in Refs. [9, 32], and y_t was taken to be 1.587 [4, 5].

Table 3: Separate fits of the dimensionless ratio Q for the six models. Columns 2 to 4 show the estimated critical coupling, the asymptotic value of Q and the amplitude of the finite-size correction due to the irrelevant field, with the irrelevant exponent fixed at $y_1=-0.82$. Some data for small system sizes, namely $L < 6, 6, 6, 8, 10$ and 10 for models 1 to 6 respectively, were excluded from these fits. Columns 5 and 6 show the value of the irrelevant exponent when left free, and the corresponding value of Q . This did not lead to meaningful results for model 4. The minimum system sizes used for these fits were $L=4$ for models 1, 2 and 3, $L=5$ for model 5, and $L=8$ for model 6. The error estimates shown between parentheses are one standard deviation.

model	K_c	$Q^{(0)}$	b_1	y_1	Q_{free}
1	0.57371376(6)	0.62339(4)	0.1183(7)	-0.83(2)	0.6235(1)
2	0.36973981(4)	0.62341(3)	0.1139(6)	-0.85(2)	0.6236(1)
3	0.22165458(2)	0.62346(2)	0.0930(4)	-0.82(2)	0.6235(1)
4	0.39342218(4)	0.62349(4)	-0.0033(5)	-	-
5	0.043038238(4)	0.62336(3)	-0.1112(5)	-0.76(2)	0.6239(2)
6	0.034326876(6)	0.62327(6)	-0.216(1)	-0.75(2)	0.6240(3)

The data for some small system sizes were excluded from these fits because additional corrections are troublesome in such small systems, as becomes apparent from the residual χ^2 . The results for K_{cj} , $Q^{(0)}$ and b_{1j} as obtained from these fits are shown in Table 3. In addition

we show results of fits with y_1 as a free parameter, for y_1 as well as for the resulting value of the universal ratio denoted Q_{free} . The statistical errors are shown between parentheses as one standard deviation in the last decimal place.

The agreement among the results in Table 3 for the universal quantities Q and y_1 is obviously less than perfect. The results for $Q^{(0)}$ and y_1 display a systematic dependence on the amplitude b_1 , which is a measure of the irrelevant field. For $Q^{(0)}$ this dependence is obviously nonlinear. The detection of this effect is a result of the higher statistical accuracy of our data in comparison with previous work [5]. The type of dependence is suggestive of the second-order term in the expansion of $Q(t, u, L)$ to u , i.e., we have to add a term $\frac{1}{2}L^{2y_1}uQ^{(0,2)}$ to Eq. (5) which amounts to including a term $b_{4j}L^{2y_1}$ in Eq. (6). Results of fits including this term, and with $y_1 = -0.82$ fixed, are shown in Table 4. They are better behaved, as visible from the χ^2 criterion, and from the absence of a systematic dependence of the results for $Q^{(0)}$ as a function of b_1 .

The results in the third column in Table 4 confirm that the six systems fit well in one common Ising universality class. Due to the additional parameter, the uncertainty margins are larger than those in Table 3, but still smaller than those of the results of Ref. [5].

Table 4: Separate fits of the dimensionless ratio Q for the six models, with a quadratic term in the irrelevant field included. Smallest system sizes included in these fits are $L = 4, 4, 4, 4, 6,$ and 8 for models 1 to 6 respectively. The last column shows the amplitude of the leading correction to scaling. It reflects the magnitude of the irrelevant field. The error estimates shown between parentheses are one standard deviation.

model	K_c	$Q^{(0)}$	b_1
1	0.57371378(7)	0.62343(8)	0.117(3)
2	0.36973981(4)	0.62350(7)	0.110(3)
3	0.22165458(2)	0.62348(5)	0.093(2)
4	0.39342218(5)	0.62343(9)	0.000(3)
5	0.043038244(4)	0.62352(6)	-0.117(2)
6	0.034326877(5)	0.62357(15)	-0.232(7)

Also included in Table 3 are the amplitudes of the corrections due to the irrelevant field of these models. Up to a constant factor these results represent the actual values of the irrelevant scaling field. As mentioned in Ref. [5], these values reflect the positions of the critical points of

these systems under a renormalization mapping on the Landau-Ginzburg-Wilson Hamiltonian of the ϕ^4 model, which is

$$\mathcal{H}(\phi)/k_B T = \int d\mathbf{x} [r\phi^2(\mathbf{x}) + v\phi^4(\mathbf{x}) + \nabla^2\phi(\mathbf{x})], \quad (7)$$

where \mathbf{x} denotes the space coordinates. The square-gradient term represents the Ising particle-particle interaction, while the parameter r is temperature-like, and v parametrizes the irrelevant field. Renormalization analysis of such a system in less than four spatial dimensions [1] shows two fixed points, one of which is located at $(r, v)=(0, 0)$ and represents the mean-field fixed point, while the other sits at nonzero values $(r^* < 0, v^* > 0)$ and represents the Ising fixed point. The crossover scaling function for the Binder ratio [35] provides a scale for the interval between both fixed points, as parametrized by the Ising irrelevant field. The determination of the amplitudes of the irrelevant corrections in Q thus determine the positions of the six models in the $(r^* < 0, v^* > 0)$ diagram shown in Fig. 2.

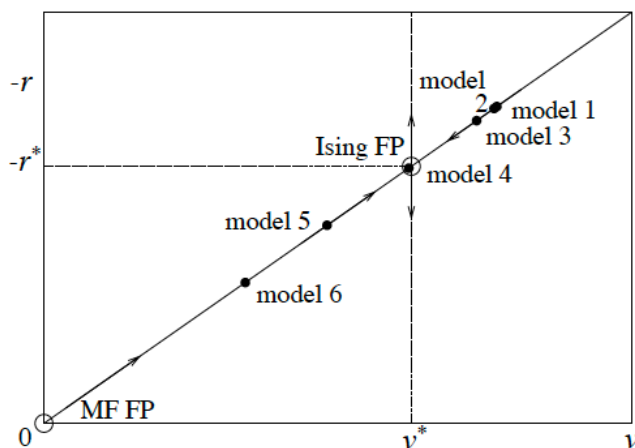


Figure 2: Sketch of positions of models 1-6 in the parameter space (r, v) of the ϕ^4 model, where r is a temperature-like parameter, and the ϕ^4 amplitude v parametrizes the irrelevant field of the Ising model. The positions of the six models are shown by black circles (\bullet). The mean-field and Ising fixed points, which are shown as open circles (\circ), are located at $(-r, v)=(0, 0)$ and $(-r^*, v^*)$, respectively.

3.2. Separate analyses of the susceptibility

Differentiation of the finite-size scaling equation for the free energy density shows that the magnetic susceptibility χ behaves as

$$\chi(t, v, L) = x(t) + L^{2y_h - d} \left(\frac{\partial h}{\partial H} \right)^2 \chi(L^{y_t} t, L^{y_1} v, 1), \quad (8)$$

Table 5: Separate fits of the susceptibility χ with the irrelevant exponent fixed at $y_1 = -0.82$. The minimum system sizes used for this fit are $L = 4, 4, 6, 4, 5$, and 8 for models 1 to 6 respectively. The error estimates shown between parentheses are one standard deviation.

model	K_c	p_1	y_h	b_1
1	0.57371380(7)	2.026(3)	2.48161(14)	-0.547(13)
2	0.36973982(5)	1.756(3)	2.48156(19)	-0.460(17)
3	0.22165459(2)	1.556(2)	2.48160(15)	-0.351(9)
4	0.39342224(5)	0.934(1)	2.48168(16)	0.004(6)
5	0.043038242(5)	0.990(1)	2.48167(13)	0.257(6)
6	0.034326874(6)	0.878(10)	2.48137(28)	0.428(13)

where the function χ on the right hand side is universal in its two remaining arguments. The contribution $x(t)$ is determined by the second derivative of the analytical part of the free energy density with respect to the physical magnetic field H . The dependence of the magnetic scaling field h on H is not universal and may, in first order, be denoted as $h = \sqrt{w_j}H$. Taylor-expansion of Eq. (8) yields

$$\begin{aligned}
\chi = & x_j + s_j(K_j - K_{cj}) & (9) \\
& + L^{2y_h-d} [p_{j0} + p_{j1}(K_j - K_{cj})L^{y_t} \\
& + p_{j2}(K_j - K_{cj})^2 L^{2y_t} + p_{j3}(K_j - K_{cj})^3 L^{3y_t} \\
& + p_{j4}(K_j - K_{cj})^4 L^{4y_t} + \sum_k b_{kj} L^{y_t} \\
& + d_j(K_j - K_{cj})L^{y_t+y_1}] ,
\end{aligned}$$

where we have used the expansion of the temperature field as in Eq. (4). The constants p_{jk} denote the product of universal expansion parameters of the function χ and nonuniversal constants including the w_j . The results of the fits for the six models are given in Table 5.

One of the variations of the fit formula included quadratic terms in the irrelevant field. This led to slightly larger values of y_h for five of the six models, although not significant in individual cases.

3.3. Separate analysis of Q_p

During the Monte Carlo simulations, also the nearest-neighbor sum e

$$e = \langle S_{nn} \rangle = \sum_{(nn)} \langle s_i s_j \rangle \quad (10)$$

was sampled. This quantity represents the interaction energy density for models 1, 2 and 4. For models 5 and 6, the nearest-neighbor sum is not the interaction energy, but it is still a quantity that scales as the energy.

Combination with the magnetization data allows the Monte Carlo sampling of the derivative $Q_p \equiv \partial Q / \partial K_{nn}$ of the Binder ratio Q with respect to the nearest-neighbor interaction. This derivative is different from that to K for models 5 and 6. It is determined by the sampled quantities as

$$\begin{aligned} Q_p &= 2 \frac{\langle m^2 S_{nn} \rangle}{\langle m^2 \rangle} - \frac{\langle m^4 S_{nn} \rangle}{\langle m^4 \rangle} - \langle S_{nn} \rangle \\ &= \frac{1}{Q} \frac{\partial Q}{\partial t} \frac{\partial t}{\partial K_{nn}}. \end{aligned} \quad (11)$$

The quantity Q_p is known [5, 9, 32] to yield fairly accurate results for the thermal exponent y_t . According to Eq. (3), the quantity Q_p behaves near the critical point as

$$Q_p(t, v, L) = L^{y_t} \frac{\partial t}{\partial K_{nn}} Q(L^{y_t} t, L^{y_1} v, 1), \quad (12)$$

Expansion of t and $\partial t / \partial K_{nn}$, and of the function Q_p in its two remaining arguments, yields

$$\begin{aligned} Q_p &= L^{y_t} [r_{j0} + r_{j1}(K_j - K_{cj})L^{y_t} \\ &+ r_{j2}(K_j - K_{cj})^2 L^{2y_t} + r_{j3}(K_j - K_{cj})^3 L^{3y_t} \\ &+ r_{j4}(K_j - K_{cj})^4 L^{4y_t} + b_{1j} L^{y_1} + d_j L^{y_2} \\ &+ c_j(K_j - K_{cj})], \end{aligned} \quad (13)$$

where we denote contributions due to the analytic part of the free energy as $d_j L^{y_2}$. The leading contribution is seen to diverge with L as L^{y_t} . This is a much stronger divergence than that of the specific heat C which displays only weakly divergent behavior as L^{2y_t-d} . Therefore, Q_p is more suitable than C to determine the temperature exponent y_t . The free parameters in Eq. (13) were fitted according to the least-squares criterion. The critical points were fixed at the values listed in Table 5. The results are shown in Table 6. They include the quantity b_1/r_0 which is proportional to the irrelevant field and may thus be compared with Tables 4 and 5.

Table 6: Separate fits of the derivative Q_p of the Binder ratio with the irrelevant exponent fixed at $y_1 = -0.82$. The minimum system sizes used for this fit are $L = 6, 6, 7, 6, 7$, and 6 for models 1 to 6 respectively. The errors quoted between parentheses are one standard deviation.

model	r_0	y_t	b_1/r_0
1	0.5302(7)	1.58674(30)	-0.082(6)
2	0.8227(8)	1.58689(21)	-0.074(4)
3	1.3529(14)	1.58710(22)	-0.057(5)
4	1.0627(13)	1.58678(28)	-0.008(5)
5	1.4224(16)	1.58713(24)	0.043(5)
6	1.4365(13)	1.58720(20)	0.086(3)

4. Simultaneous finite-size scaling analyses

4.1. Simultaneous analysis of Q

The results of Sec. 3 indicate that the six models under investigation belong to the same universality class. We thus assume that the universal parameters of these six models are exactly equal and we analyze the combined numerical data for Q of these systems simultaneously. Separation of the universal and nonuniversal constants in Eqs. (4) and (5) yields

$$\begin{aligned}
Q &= Q^{(0)} \\
&+ Q^{(1)} a_j (K_j - K_{cj}) L^{y_t} + Q^{(2)} a_j^2 (K_j - K_{cj})^2 L^{2y_t} \\
&+ Q^{(3)} a_j^3 (K_j - K_{cj})^3 L^{3y_t} + Q^{(4)} a_j^4 (K_j - K_{cj})^4 L^{4y_t} \\
&+ c_j (K_j - K_{cj})^2 L^{y_t} + b_{1j} L^{y_1} + b_{2j} L^{y_2} + b_{3j} L^{y_3} \\
&+ d_j (K_j - K_{cj}) L^{y_t + y_1},
\end{aligned} \tag{14}$$

where we abbreviated $Q^{(j,0)}$ as $Q^{(j)}$ and combined the other $Q^{(k,l)}$ with their nonuniversal prefactors into constants denoted c_j and b_{1j} . The term with amplitude c_j is due to the nonlinear dependence of the temperature field t as a function of K_j . The correction exponents y_j have the same meaning as above. On the basis of Eq. (14), least squares fits were applied to the combined data for Q of the six models. The exponents were set at the values given above,

except the irrelevant one $y_1 = y_i$ which is now treated as a free parameter. Furthermore we set $Q^{(1)} = 1$, which defines a scale of the temperature field.

In this type of simultaneous fit, the universal constants $Q^{(k)}$ and the exponents appear only once, so that the total number of free parameters is reduced appreciably. Also the effect mentioned in Sec. 1 contributes to the accuracy of the fit, in particular to that of the irrelevant exponent y_1 . The results, which are summarized in Table 7, do indeed display a substantially improved accuracy in comparison with those of the separate fits.

Table 7: Simultaneous fit of the ratio Q . The minimum system sizes that were included in this fit were $L=6$ for models 1-5 and $L=8$ for model 6. The error margins quoted between parentheses are two standard deviations.

y_1	$Q(0)$	$Q(1)$	$Q(2)$	$Q(3)$	$Q(4)$
-0.821(5)	0.62356(5)	1 (fixed)	0.85(3)	-3.2(2)	-6.0(27)
$K_c^{(1)}$	$K_c^{(2)}$	$K_c^{(3)}$	$K_c^{(4)}$	$K_c^{(5)}$	$K_c^{(6)}$
0.57371386(9)	0.36973988(6)	0.22165461(3)	0.39342221(6)	0.043038246(7)	0.034326877(5)
a_1	a_2	a_3	a_4	a_5	a_6
0.329(2)	0.5115(14)	0.844(4)	0.664(2)	4.04(4)	4.98(5)
b_{11}	b_{12}	b_{13}	b_{14}	b_{15}	b_{16}
0.1124(17)	0.1088(17)	0.0897(14)	-0.0050(9)	-0.119(4)	-0.233(8)

4.2. Simultaneous analysis of χ

We rewrite the parameters p_{jk} in the right-hand side of Eq. (9) as the product of universal expansion parameters $\chi^{(k)}$ of the function χ in its first argument, and nonuniversal expansion parameters a_j . Then Eq. (9) changes into

$$\begin{aligned}
\chi &= x_j + s_j(K_j - K_{cj}) + L^{2y_h - d} w_j [\chi^{(0)} \\
&+ \chi^{(1)} a_j (K_j - K_{cj}) L^{y_t} + \chi^{(2)} a_j^2 (K_j - K_{cj})^2 L^{2y_t} \\
&+ \chi^{(3)} a_j^3 (K_j - K_{cj})^3 L^{3y_t} + \chi^{(4)} a_j^4 (K_j - K_{cj})^4 L^{4y_t} \\
&+ b_j L^{y_j} + c_j (K_j - K_{cj}) L^{y_t + y_1} + \dots],
\end{aligned} \tag{15}$$

where we have expanded the temperature field as $t = a_j(K_j - K_{cj}) + b_j(K_j - K_{cj})^2 + \dots$.

Fits were made to the Monte Carlo data for χ on the basis of Eq. (15). The results are presented in Table 8. Just as for Q , the scale of the temperature and magnetic scaling fields may be chosen freely so that we may fix two parameters, namely $\chi^{(0)}=\chi^{(1)}=1$ in Eq. (15) during the fit. Again the reduction of the number of free parameters is accompanied by an improved accuracy of the results in comparison with the separate fits.

Table 8: Simultaneous fit of the magnetic susceptibility χ with the temperature exponent fixed at $y_t=1.587$ and the irrelevant exponent at $y_1 = -0.82$. Also the first two expansion parameters were fixed at $\chi^{(0)}=1$ and $\chi^{(1)}=1$. Errors are quoted as one sigma.

y_h	$\chi^{(0)}$	$\chi^{(1)}$	$\chi^{(2)}$	$\chi^{(3)}$	$\chi^{(4)}$
2.48178(5)	1 (fixed)	1 (fixed)	-0.13(2)	0.82 (fixed)	1.587 (fixed)
$K_c^{(1)}$	$K_c^{(2)}$	$K_c^{(3)}$	$K_c^{(4)}$	$K_c^{(5)}$	$K_c^{(6)}$
0.57371386(4)	0.36973989(3)	0.22165462(2)	0.39342222(3)	0.043038244(3)	0.034326881(3)
w_1	w_2	w_3	w_4	w_5	w_6
2.023(1)	1.7530(8)	1.5509(7)	0.9328(4)	0.9886(5)	0.8746(4)
a_1	a_2	a_3	a_4	a_5	a_6
1.31(1)	1.989(3)	3.28(1)	2.606(5)	16.0(2)	19.4(1)

4.3. Simultaneous analysis of Q_p

Separation of the universal parameters following from the expansion of the universal function Q_p in Eq. (12) and the nonuniversal ones yields

$$\begin{aligned}
Q_p &= L^{y_t} p_j [Q_p^{(0)} + Q_p^{(1)} a_j (K_j - K_{cj}) L^{y_t} \\
&+ Q_p^{(2)} a_j^2 (K_j - K_{cj})^2 L^{2y_t} + Q_p^{(3)} a_j^3 (K_j - K_{cj})^3 L^{3y_t} \\
&+ Q_p^{(4)} a_j^4 (K_j - K_{cj})^4 L^{4y_t} + b_j L^{y_1} + d_j L^{y_t - y_1} \\
&+ e_j (K_j - K_{cj}) L^{y_1 + y_t} + c_j (K_j - K_{cj})],
\end{aligned} \tag{16}$$

where the universal parameters $Q_p^{(k)}$ are determined by the function Q_p . The nonuniversal parameters p_j are defined as $\partial t / \partial K_{nn}$ for the j -th model. As above we took the critical points

from Table 7 as fixed parameters in the fitting procedure. The results of these least-squares fits of Eq. (16) to the Monte Carlo results appeared to depend only weakly on the precise value of the critical points. The results are shown in Table 9.

We performed several variations of this procedure. For instance we included a term proportional to $L^{y_1}(K_j - K_{cj})$ in the square brackets of Eq. (16). However, this did not lead to a clear reduction of the residual χ^2 of the fit. The uncertainty margins shown in Table 9 include the variations due to different procedures, and the dependence on the cutoff at small system sizes.

Table 9: Result of simultaneous fit of Q_p . One sigma errors are shown between parentheses.

y_t	$Q_p(0)$	$Q_p(1)$	$Q_p(2)$	$Q_p(3)$	$Q_p(4)$
1.58693(9)	1 (fixed)	0.1 (fixed)	-9(2)	-7(3)	53(25)
a_1	a_2	a_3	a_4	a_5	a_6
-0.35(4)	-0.54(7)	-0.89(11)	-0.71(9)	-4.4(5)	-5.2(6)
p_1	p_2	p_3	p_4	p_5	p_6
0.5298(2)	0.8227(3)	1.3543(6)	1.0622(5)	1.4238(6)	1.4391(6)

5. Discussion

By means of an analysis of extensive Monte Carlo simulations of six three-dimensional Ising-like models, we have succeeded in refining the results for several universal constants of the Ising universality class. Furthermore, the margins for deviations from universality between the six models are reduced, which is significant because a rigorous basis for universality is still lacking. The present confirmation of universality is in line with earlier findings [5, 36].

Furthermore the results obtained in the simultaneous fit allow an additional confirmation of universality. As noted above, the derivative a_i of the temperature field to the coupling of the i -th model occurs in the expansion of Q as well as in that of χ . They differ only because they are expressed in different units. Thus, according to universality, the ratios between the amplitudes a_i of Q , χ and Q_p should be model-independent. Table 10 accordingly displays the $a_i^{(Q)}/a_i^{(\chi)}$ and $a_i^{(Q)}/a_i^{(Q_p)}$ for the six models. The results are in a good agreement with universality. Table 10 includes the ratio $a_i^{(Q)}/p_i^{(Q_p)}$, which may be expected to be constant only

for models 1 to 4, because the amplitudes p_i involve differentiation to K_{nn} while $K \neq K_{nn}$ for models 5 and 6.

Table 10: Results for the amplitude ratios $a_i^{(Q)}/a_i^{(\chi)}$, $a_i^{(Q)}/a_i^{(Q_p)}$ and $a_i^{(Q)}/p_i^{(Q_p)}$, where the superscripts refer to the expansion parameters used in the fits for Q , χ and Q_p . Theory predicts entries to be equal on each line, except for models 5 and 6 on line 3.

model	1	2	3	4	5	6
$a_i^{(Q)}/a_i^{(\chi)}$	0.253(3)	0.257(1)	0.257(1)	0.255(1)	0.253(3)	0.257(3)
$a_i^{(Q)}/a_i^{(Q_p)}$	-0.93(10)	-0.94(11)	-0.95(11)	-0.94(11)	-0.92(11)	-0.96(12)
$a_i^{(Q)}/p_i^{(Q_p)}$	0.621(4)	0.622(2)	0.623(3)	0.625(2)	2.84(3)	3.46(4)

The improvement of the results in comparison with Ref. [5] is based on better statistical accuracies, and simulation of larger systems of size $L = 256$. The six models were selected such that the irrelevant field covers a wide range. On the one side of this range we have the model on the hydrogen peroxide lattice with only 3 nearest neighbors, and on the other side of the scale we have the equivalent-neighbor model on the simple-cubic lattice with four layers of neighbors, which is, as illustrated in Fig. 2, relatively close to the mean-field model in terms of crossover between the mean-field and Ising fixed points. In agreement with earlier findings, the simultaneous analysis of the Monte Carlo data helps to reduce the uncertainty margins, especially for the errors of the irrelevant exponent y_1 and of quantities, like the Binder ratio Q , that are sensitive to the value of y_1 .

The reduction of the error margins in our final results is not a simple and direct result of the better statistics of the Monte Carlo data. Reduction of the statistical errors can reveal new corrections to the leading scaling behavior that were below the detection threshold in earlier analyses. For instance, this applies to the correction term with exponent $y_1 - y_t$ in the analysis of Q_p . Since the addition of new free parameters in the fit formula typically increases the statistical error margins of the results, the improvement of the results is less than expected on the basis of statistics only. Another problem with a similar effect is that the cutoff at small systems may have to be chosen at a larger value of L .

Our results are summarized in Tables 11 and 12. These tables also include some existing

results for easy comparison. The most recent estimate of the critical point using Monte Carlo Renormalization Group [37] $K_c = 0.2216547(1)$.

Table 11: Comparison between present results and existing values for the critical points. Errors quoted are two sigma.

model	K_c (present)	K_c (Ref. [5])	K_c (other refs.)	K_c (other refs.)
1	0.57371385(9)	-	0.573795(16)	[16] -
2	0.36973987(6)	0.36973980(9)	0.36978(4)	[40] 0.3697(8) [41]
3	0.22165459(3)	0.22165455(5)	0.221655(2)	[42] 0.221654628(2) [50]
3	-	-	0.221654626(5)	[51] 0.221654631(8) [55]
4	0.39342220(6)	0.39342225(9)	0.3934220(7)	[9] -
5	0.043038246(7)	0.0430381(4)	0.0430381(4)	[35] 0.0432 [44]
6	0.034326877(5)	0.03432687(2)	0.03432685(15)	[35] -

While most of the new results agree well with those of Ref. [5], the result for $Q^{(0)}$ differs more than the combined error bounds. This is mostly due to the second-order term in the expansion of Q in the irrelevant field which is now included. This term also explains the difference of the new result $y_h = 2.48178(5)$ with that of Ref. [5], which slightly exceeds the combined error margins. It is quite satisfactory to observe that the present results for the Ising universal parameters, obtained by different methods as renormalization, series expansions and Monte Carlo, coincide within narrow margins. Also the results for nonuniversal quantities, such as the critical points as obtained by different methods are, in most cases, in an excellent agreement. There is a small discrepancy of our result $K_c = 0.57371385(9)$ for the critical point of the hydrogen peroxide lattice model with the series-expansion result [16] $K_c = 0.573795(16)$, which may be related to the large value of the irrelevant field in this model. Our result is in accurate agreement with a very recent independent result obtained by Liu et al. [38] using a worm algorithm. More serious discrepancies exist with results of a conjectured exact solution of the three-dimensional Ising model by Zhang [39]. His result for the critical point of the simple-cubic Ising models lies several orders of magnitude outside the mutually consistent estimated error margins of independent results [5]. In this context it relevant to mention that Wu et

al. [53] and Perk [43] pointed out several errors in Ref. [39] that invalidate all its main results.

6. Acknowledgments

We are indebted to Dr. A. L. Talapov for his contributions to the Cluster Processor in the early stages of this project, and to Dr. J. R. Heringa for valuable discussions. The construction of the Cluster Processor was funded by the NWO (“Nederlandse Organisatie voor Wetenschappelijk Onderzoek”) via grants 047-13-210 and 047-003-019. YD was supported by National Natural Science Foundation of China (Grant No. 12275263) and the Natural Science Foundation of Fujian Province of China (Grant No. 2023J02032). LNS was supported by the Russian Science Foundation (Grant 25-11-00158).

References

- [1] K.G. Wilson and M.E. Fisher, *Phys. Rev. Lett.* 28, 240 (1972).
- [2] J.C. Le Guillou and J. Zinn-Justin, *J. Physique* 48, 19 (1987).
- [3] R. Guida and J. Zinn-Justin, *J. Phys. A* 31, 8103 (1998).
- [4] M. Campostrini, A. Pelissetto, P. Rossi, and E. Vicari, *Phys. Rev. E* 65, 066127 (2002).
- [5] Y. Deng and H.W.J. Blöte, *Phys. Rev. E* 68, 036125 (2003).
- [6] A. Yamagata, *Physica A* 222, 119 (1995).
- [7] A. Yamagata, *Physica A* 231, 495 (1996).
- [8] J. García, J.A. Gonzalo, and M.I. Marqués, preprint, cond-mat/0211270.
- [9] H.W.J. Blöte, E. Luijten, and J.R. Heringa, *J. Phys. A* 28, 6289 (1995).
- [10] H.W.J. Blöte, J.R. Heringa, A. Hoogland, E.W. Meyer, and T.S. Smit, *Phys. Rev. Lett.* 76, 2613 (1996).
- [11] M. Blume, *Phys. Rev.* 141, 517 (1966).
- [12] H.W. Capel, *Physica A* 32, 966 (1966); *Phys. Lett.* 23, 327 (1966).

Table 12: Comparison between the present results for the renormalization exponents and the universal ratio $Q^{(0)}$ for the three-dimensional Ising universality class and literature values. The methods to obtain these results are abbreviated as follows: RG – renormalization of ϕ^4 model; HTE – high-temperature series expansion; MC – Monte Carlo and finite-size scaling; MCRG – Monte Carlo renormalization; CAM – coherent-anomaly method.

Refs.	Year	y_t	y_h	y_1	$Q^{(0)}$	Method
Le Guillou et al. [2]	1980	1.587(4)	2.485(2)	-0.79(3)		RG
Nickel and Rehr [45]	1990	1.587(4)	2.4821(4)	-0.83(5)		HTE
Nickel [46]	1991	1.587	2.4823	-0.84		HTE
Baillie et al. [47]	1992	1.602(5)	2.4870(15)	-0.825(25)		MCRG
Landau [48]	1994	1.590(2)	2.482(7)			MC
Kolesik et al. [49]	1995	1.586(4)	2.482(4)			CAM
Blöte et al. [9]	1995	1.587(2)	2.4815(15)	-0.82(6)	0.6233(4)	MC
Blöte et al. [10]	1996	1.585(2)	2.4810(10)			MCRG
Guida et al. [3]	1998	1.586(3)	2.483(2)	-0.799(11)		RG
Blöte et al. [32]	1999	1.5865(14)	2.4814(5)	-0.82(3)	0.62358(15)	MC
Campostrini et al. [4]	2002	1.5869(4)	2.48180(15)	-0.82(5)		HTE
Deng and Blöte [5]	2003	1.5868(3)	2.4816(1)	-0.821(5)	0.62341(4)	MC
Butera and Comma [42]	2005	1.5870(5)	2.4818(4)			HTE
Hasenbusch [50]	2010	1.58725(22)		-0.832(6)		MC
Rychkov [56, 57]	2016	1.58737(8)	2.48072(62)			MC
Ferrenberg et al. [51]	2018	1.58752(22)	2.48195(6)			MC
Hasenbusch [52]	2021	1.58739(7)		-0.825(20)		MC
Ron et al. [37]	2021		2.4824(1)			MCRG
Present	2011	1.58693(9)	2.48178(5)	-0.821(5)	0.62355(5)	MC

- [13] E. Luijten, H.W.J. Blöte and K. Binder, *Phys. Rev. E* 54, 4626 (1996).
- [14] B. Nienhuis, A.N. Berker, E.K. Riedel and M. Schick, *Phys. Rev. Lett.* 43, 737 (1979).
- [15] A.L. Talapov, H.W.J. Blöte and L.N. Shchur, *Pisma v ZhETF* 62, 157 (1995); *JETP Lett.* 62, 174 (1995).
- [16] J.A. Leu, D.D. Betts and C.J. Elliott, *Can. J. Phys.* 47, 1671 (1969).
- [17] E. Domany, D. Mukamel, B. Nienhuis and A. Schwimmer, *Nucl. Phys. B* 190 [FS3], 279 (1981).
- [18] A. Hoogland, J. Spaa, B. Selman and A. Compagner, *J. Comp. Phys.* 51, 250 (1983).
- [19] M.N. Barber, R.B. Pearson, D. Toussaint and J.L. Richardson, *Phys. Rev. B* 32, 1720 (1985).
- [20] G. Parisi and F. Rapuano, *Phys. Lett. B* 157, 301 (1985).
- [21] A. Hoogland, A. Compagner and H.W.J. Blöte, *Physica A* 132, 593 (1985).
- [22] G. Bhanot, D. Duke and R. Salvador, *Phys. Rev. B* 33, 7841 (1986).
- [23] A. Hoogland, A. Compagner and H.W.J. Blöte, *The Delft Ising System Processor*, Chapter 7 of *Architecture and Performance of Specialized Computers*, ed. B. Alder, in the series *Computational Techniques* (Academic, New York, 1988).
- [24] A.M. Ferrenberg, D.P. Landau and Y.J. Wong, *Phys. Rev. Lett.* 69, 3382 (1992).
- [25] L.N. Shchur and H.W.J. Blöte, *Phys. Rev. E* 55, 4905R (1997).
- [26] L.N. Shchur, J.R. Heringa, and H.W.J. Blöte, *Physica A* 241, 579 (1997).
- [27] W. Selke, A.L. Talapov, L.N. Shchur, *JETP Lett.*, 58, 665 (1993).
- [28] U. Wolff, *Phys. Rev. Lett.* 60, 1461 (1988).
- [29] A.L. Talapov and H.W.J. Blöte, *J. Phys. A* 29, 5727 (1996).
- [30] X.S. Chen, V. Dohm and A.L. Talapov, *Physica A* 232, 375 (1996).

- [31] L. Shchur, *Physics-Uspekhi* 55, 733 (2012).
- [32] H.W.J. Blöte, L.N. Shchur, and A.L. Talapov, *Int. J. Mod. Phys. C* 10, 1137 (1999).
- [33] K. Binder, *Z. Phys. B* 43, 119 (1981).
- [34] E. Luijten, *Interaction Range, Universality and the Upper Critical Dimension* (Delft University Press, 1997), p.16.
- [35] E. Luijten, *Phys. Rev. E* 59, 4997 (1999).
- [36] P. Butera and M. Comi, *Phys. Rev. B* 69, 174416 (2004).
- [37] D. Ron, A. Brandt, and R.H. Swendsen, *Phys. Rev. E* 104, 025311 (2021).
- [38] Q. Liu, Y. Deng, T.M. Garoni, H.W.J. Blöte, *Nucl. Phys. B* 859, 107 (2012).
- [39] Z.-D. Zhang, *Philos. Mag.* 87, 5309 (2007).
- [40] M.F. Sykes and D.S. Gaunt, *J. Phys. A* 6, 643 (1973).
- [41] O.G. Mouritsen, *J. Phys. C* 13, 3909 (1980).
- [42] P. Butera and M. Comi, *Phys. Rev. B* 72, 14442 (2005).
- [43] J.H.H. Perk, *Philos. Mag.* 89, 761 (2009).
- [44] C. Domb and N.W. Dalton, *Proc. Phys. Soc. London* 98, 859 (1966).
- [45] B.G. Nickel and Rehr, *J. Stat. Phys.* 61, 1 (1990).
- [46] B.G. Nickel, *Physica A* 177, 189 (1991).
- [47] C.F. Baillie, R. Gupta, K.A. Hawick, and G.S. Pawley, *Phys. Rev. B* 45, 10438 (1992).
- [48] L.D. Landau, *Physica A* 205, 41 (1994).
- [49] M. Kolesik and M. Suzuki, *Physica A* 215, 138 (1995).
- [50] M. Hasenbusch, *Phys. Rev. B* 82, 174433 (2010).
- [51] A.M. Ferrenberg, J. Xu, and D.P. Landau, *Phys. Rev. E* 97, 043301 (2018).

- [52] M. Hasenbusch, Phys. Rev. B 104, 014426 (2021).
- [53] F.Y. Wu, B.M. McCoy, M.E. Fisher and L. Chayes, Phil. Mag. 88, 3093 (2008).
- [54] C.J. Thompson and A.J. Guttmann, Phys. Lett. A 53, 315 (1975).
- [55] P. Hou, S. Fang, J. Wang, H. Hu, and Y. Deng, Rev. E 99, 042150 (2019).
- [56] S. El-Showk, M.F. Paulos, D. Poland, S. Rychkov, D. Simmons-Duffin, and A. Vichi, Phys. Rev D 86, 025022 (2012).
- [57] S. Rychkov, Comptes Rendus Physique, 21, 185 (2020).